An Efficient 3D Model of Heterogeneous Materials for Elastic Contact Applications Using Multigrid Methods

H. Boffy, Marie-Christine Baietto, P. Sainsot, Ton Lubrecht

An Efficient 3D Model of Heterogeneous Materials for Elastic Contact Applications Using Multigrid Methods

Hugo Boffy[1]
Ph.D. Student
LaMCoS, CNRS UMR 5259,
Université de Lyon, INSA-Lyon,
Villeurbanne, F69621, France
e-mail: hugo.boffy@insa-lyon.fr

Marie-Christine Baietto
CNRS Research Director
LaMCoS, CNRS UMR 5259,
Université de Lyon, INSA-Lyon,
Villeurbanne, F69621, France
e-mail: marie-christine.baietto@insa-lyon.fr

Philippe Sainsot
Assistant Professor
LaMCoS, CNRS UMR 5259,
Université de Lyon, INSA-Lyon,
Villeurbanne, F69621, France
e-mail: philippe.sainsot@insa-lyon.fr

Antonius A. Lubrecht
Professor
LaMCoS, CNRS UMR 5259,
Université de Lyon, INSA-Lyon,
Villeurbanne, F69621, France
e-mail: ton.lubrecht@insa-lyon.fr

A 3D graded coating/substrate model based on multigrid techniques within a finite difference frame work is presented. Localized refinement is implemented to optimize memory requirement and computing time. Validation of the solver is performed through a comparison with analytical results for (i) a homogeneous material and (ii) a graded material. The algorithm performance is analyzed through a parametric study describing the influence of layer thickness ($0.01 < t/a < 10$) and mechanical properties ($0.005 < E_c/E_s < 10$) of the coating on the contact parameters (P_h, a). Three-dimensional examples are then presented to illustrate the efficiency and the large range of possibilities of the model. The influence of different gradations of Young's modulus, constant, linear and sinusoidal, through the coating thickness on the maximum tensile stress is analyzed, showing that the sinusoidal gradation best accommodates the property mismatch of two successive layers. A final case is designed to show that full 3D spatial property variations can be accounted for. Two spherical inclusions of different size made from elastic solids with Young's modulus and Poisson's ratio are embedded within an elastically mismatched finite domain and the stress field is computed.

1 Introduction

The actual contact between solid surfaces is generally rough and the stresses induced can only be correctly described using a detailed 3D model. Current manufacturing processes allow one to obtain functional graded materials, i.e., materials with 3D varying properties. A traditional application is a coated material. Nevertheless, the rough coated contact problem is strongly multi-scale: the characteristic dimensions of the contact, the coating and the roughness range from the millimeter to the nanometer. A straightforward discretization of this multi-scale problem would exceed the memory and CPU capacity of current (and next generation) computers. This paper proposes an efficient numerical model that can handle such multi-scale problem requiring $O(10^9)$ points and locally refined grids.

The development and coating selection becomes a complex and costly task for designers. Numerical simulations can thus guide the choice of the designer and reduce the cost of an experimental approach. Substrate and coating are generally elastically dissimilar; thus the contact stresses and the internal stresses will differ from those generated in the uncoated case and quantification is necessary. The actual stress distribution is mostly calculated using numerical or semi-numerical techniques for layered materials. These numerical simulations can become very difficult when varying properties and thin coatings are involved. These computations can aid in fine tuning the material choice to the specific operating conditions, such as layer thickness, property variations, etc. Several studies have been performed on this topic and will be outlined later on.

Most of the models consider discrete isotropic layers with constant properties and a sharp transition at the interface. Moreover, perfect bounds at interfaces are assumed and this leads to inherent stress discontinuities at the interface. The methods used are generally based on integral transform combined with a Fast Fourier Transform (FFT) algorithm or on Finite Element (FE) methods.

Ju and Liu [1] and Leroy et al. [2] used the Fourier transform to study the thermo-mechanical deformation of a 2D layered elastic half space subjected to a moving heat source. Plumet and Dubourg [3] used these techniques to study the 3D mechanical case. FFT methods introduce a numerical periodicity error which can vanish if one extends the surface grid sufficiently far beyond the contact area. In their work, Polonsky and Keer [4,5] remedy the periodicity error by using a special correction term. Nogi and Kato [6] combined the conjugate gradient method with the FFT technique for solving the rough contact problem for both homogeneous and layered solids. FFT methods can deal with coated materials but are not appropriated for graded ones when property variations do not follow a single space direction.

Kesler et al. [7,8] worked on experimental methods to determine the residual stresses and the intrinsic stresses resulting from the deposition process. They also studied the Young's modulus of a layered or graded material as a function of depth in the deposit. Giannakopoulos and Suresh [9] developed semi-analytical models to adress graded materials with properties varying either as exponential or power laws. More recently, Prasad et al. [10] studied the steady-state frictional sliding contact on surfaces of plastically graded materials using FE techniques.

In 3D mechanical studies, simulations are mostly performed using FE techniques [11,12]. Holmberg et al. [11] used these methods to calculate the real stress components and fracture toughness of a coated surface and to investigate the effect of residual stress in the coating. This approach presents a major disadvantage for thin layers, which is the large system of equations arising from the fine mesh. Conventional numerical methods take unacceptably long times even on modern computers. The computation speed can be increased by using advanced numerical techniques such as multigrid methods [13].

Semi-analytical methods have also been used in the case of graded and coated materials to determine displacement and stress fields. Fretigny et al. [14] developed an analytical approach to the mechanics of adhesive contacts between coated substrates and

rigid axisymmetric probes as an extension of a model developed by Perriot [15] for the non-adhesive case. Giannakopoulos and Suresh [9] studied the stresses in the case of a graded material with an exponential variation of its Young's modulus in depth. The methods used cannot deal with all types of variations.

Watremetz et al. [16] developed a 2D thermomechanical numerical model based on multigrid methods to solve mechanical problems including both coated and graded materials. His model is able to solve problems with any type of property variation. He particularly showed how a graded variation avoids the discontinuity in the stress components.

Starting from Ref. [16], extensions were realized to propose a 3D multigrid model for homogeneous bodies submitted to a moving heat source [17]. Then a 3D multigrid elastic contact model for coated and graded materials with 3D spatial property variations has been developed. This work is based on the finite difference method which allows one to account for property variations in all space dimensions. A local refinement strategy is used to reduce computation time.

The model is presented in the first section. The validation is outlined in Sec. 2. Comparisons are performed with classical Hertzian solutions given by Johnson [18] and analytical solutions proposed by Giannakopoulos and Suresh [9]. In Sec. 3, a parametric study of a coated substrate is conducted. A large range of coating thickness and E_c/E_s ratio is considered to illustrate the efficiency and robustness of the model. Three-dimensional numerical examples are then presented in Sec. 4 to illustrate the efficiency and the large range of possibilities of the model. Coating/substrate systems with different property gradations through the coating thickness, constant, linear and sinusoidal, are submitted to contact loading. The resulting stress fields within the coating and the substrate and at the interface are analyzed. A final case is then designed to show that full 3D spatial property variations can be accounted for. Two spherical inclusions of different size made from different materials (a compliant and a stiff one) are embedded within an elastically mismatched finite domain. The stress field is computed.

2 3D Model and Numerical Method

3D Numerical tools dealing with coating problems are generally based on Finite Element Methods (FEM) or on semi-analytical techniques combined with Fast Fourier Transform (FFT). FEM demand a huge computational effort (CPU and memory) if one requires locally very fine meshes. FFT methods cannot deal with three-dimensional varying mechanical properties. A finite difference discretization can handle such three-dimensional varying properties, but requires rather important computational efforts. Using multigrid methods (MG) the convergence speed can be accelerated and large scale problems can be solved with a limited computational effort. Moreover, these methods can easily be coupled with mesh refinement strategies allowing one to deal with the different contact scales [13,19].

The first to apply these techniques to a 2D elastic model was Watremetz et al. [16]. He studied a material with graded transverse elastic properties.

2.1 Equations. The work is based on a second order finite difference formulation of 3D Lamé equations, written for a finite rectangular domain. The Lamé coefficients can vary as a function of space, i.e., $\lambda = f(x,y,z)$, $\mu = g(x,y,z)$. Hence the Young's modulus and Poisson's ratio of this elastic solid are obviously 3D spatial varying functions ($E(x,y,z)$,$\nu(x,y,z)$). Thus any property gradation can be accounted for through the depth, but also along x and y directions. Applications like embedded inclusions within a mismatched elastic solid can be addressed as it will be shown in Sec. 4. These equations can be generalized in terms of displacements ($u(x,y,z)$) to:

$$(\lambda u_{j,j})_{,i} + (\mu u_{i,j})_{,j} + (\mu u_{j,i})_{,j} = 0 \quad i,j = 1,2,3 \tag{1}$$

The partial differential equations PDE are discretized using a second order finite difference scheme in the bulk except on the boundaries. One of the originalities of this work is that the cross derivative terms are taken into account as $\frac{\partial}{\partial x}\left(\lambda\frac{\partial u}{\partial x}\right)$ due to the property variations along all spatial dimensions.

Displacements are determined using boundary conditions (BC). Dirichlet BC (displacements) are imposed on the five boundaries and Neuman BC prescribe the load on the top free surface according to the following equation:

$$\begin{cases} \sigma_{zz} = \lambda\left(\dfrac{\partial w}{\partial z} + \dfrac{\partial v}{\partial y} + \dfrac{\partial u}{\partial x}\right) \\ \sigma_{zy} = \mu\left(\dfrac{\partial w}{\partial y} + \dfrac{\partial v}{\partial z}\right) \\ \sigma_{zx} = \mu\left(\dfrac{\partial w}{\partial x} + \dfrac{\partial u}{\partial z}\right) \end{cases} \tag{2}$$

2.2 Multigrid Methods. Conventional iterative methods converge slowly as the long wavelength error present in the solution slowly diminishes with successive relaxation sweeps. Multigrid techniques overcome this difficulty by using a sequence of grids. The grids communicate with one another through restriction and prolongation operators [20,21]. Efficient multigrid algorithms for the solution of PDE require good ellipticity, which implies that non-smooth error components can be solved by local processing. The elasticity equations are elliptic and one can expect a good multigrid efficiency. The treatment of the Dirichlet BC is straight forward, however, Neumann BC can seriously degrade the solver efficiency.

2.3 Boundary Conditions. The boundary conditions should not modify the efficiency of the multigrid techniques. The Dirichlet conditions are easily implemented. Concerning the Neumann ones, in order to maintain the multigrid solver efficiency, the BC have to fulfil two criteria:

- consistency on the various grids
- no introduction of local errors.

Venner and Lubrecht [13] relax the interior problem on the surface using the Neumann condition to fulfill both criteria. Some pre-relaxations are necessary to decrease the residual near the boundaries before solving the entire problem, as described by Brandt [21].

2.4 Refinement Strategy. Coated and graded systems are multi-scale problems as a large difference between coating thickness, loaded zone and the substrate dimensions exists. A uniform level of resolution is not required everywhere and a proper spatial resolution, fine for instance around the coating and the interface and coarse elsewhere, allows a considerable reduction of the computational work. This is especially true if one considers a coated semi-infinite bulk (bulk size $\gg$ coating thickness and/or contact width). MG techniques are easily combined with local mesh refinements techniques. In such cases, the finest grids can be restricted to smaller and smaller subdomains, whereas the coarse grids cover the entire domain.

The refinement strategy consists in defining successive subdomains corresponding to successive levels where grid refinement is performed only locally (Fig. 1). The fine grid residuals and the coarse grid correction are only carried out in the local part where the fine grid exists [19]. The refinement strategy is centered on M (0,0,0). A refined level corresponds to a reduction of the coarsen volume with a ratio of 3/4 in the x and y directions and 1/2 in the z direction. The 1/2 z-ratio allows one to maintain a constant number of grid-points along the z direction. In order to show the efficiency of the refinement strategy, a simple case is studied. A Hertzian loading is imposed at the surface of a rectangular domain. Numerical simulations are conducted with a different

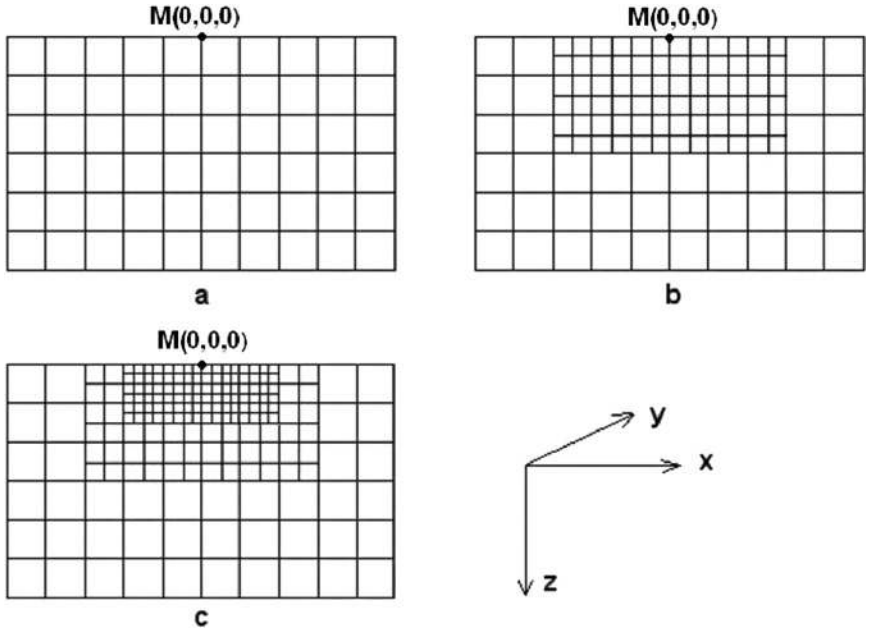

Fig. 1 Local refinement technique: (*a*) coarsen grid, (*b*) one-level local refinement, (*c*) two-level local refinement

number of levels of local refinement, from a one-level to six-level local refinements. The case considered as the reference includes six grid levels and no local refinement (number of grid-points on the finest grid around 67M and u_{ref} the reference solution). This number of grid-points reduces drastically, down to 14K for the five-level local refinement case. The difference between the reference solution u_{ref} and the solution u_{app} obtained using p-level local grid refinement and the corresponding reduction in computational time, are summarized in Table 1. A maximum and a mean displacement error norm are defined respectively as:

$$\left\|u_{\text{ref}} - u_{\text{app}}\right\|_{\infty} = \max\left(\left\|\frac{u_{\text{ref}} - u_{\text{app}}}{u_{\text{ref}}}\right\|\right)$$

$$\left\|u_{\text{ref}} - u_{\text{app}}\right\|_{1} = \frac{1}{N}\sum_{0}^{N}\left(\frac{\left\|u_{\text{ref}} - u_{\text{app}}\right\|}{u_{\text{ref}}}\right)$$

The maximum error increases with increasing number of local refined levels, but the accuracy remains pretty good. The time reduction increases very significantly with the increasing number of local refined levels and the calculation can be performed up to 300 times faster with almost the same accuracy in this case. These results show the ability of the model to deal with local refinement techniques combined with MG. This was required to address large 3D problems requiring high resolution sub-domains.

3 Validation

The next step consists in validating the model and illustrating its accuracy. Three problems are considered and the numerical results are compared with analytical solutions to validate (i) the multigrid model, (ii) the contact solution within the multigrid framework, and (iii) the description of coatings with elastic property gradients through the depth. Calculations based on multigrid techniques were performed using different number of levels without local refinement, ranging from 1 (monogrid) to 7 grid levels. A rectangular domain is considered of length $L_x/a = L_y/a = 2 * L_z/a = 16$. The coarse grid involves 9*9*5 points and the finest one 513*513*257 points with a mesh size of 1/32.

Table 1 Computational time reduction and accuracy of the solver versus the number of p-level local refinements

p	$\left\|u_{\text{ref}} - u_{\text{app}}\right\|_{\infty}$	$\left\|u_{\text{ref}} - u_{\text{app}}\right\|_{1}$	Time reduction
1	$6.8 * 10^{-5}$	$3.6 * 10^{-5}$	3.0
2	$2.8 * 10^{-4}$	$1.6 * 10^{-5}$	10.0
3	$6.2 * 10^{-4}$	$3.2 * 10^{-4}$	34.5
4	$1.5 * 10^{-3}$	$5.0 * 10^{-4}$	142.8
5	$2.1 * 10^{-3}$	$6.5 * 10^{-4}$	384.6

3.1 Multigrid Model Validation. A homogeneous bulk submitted to an Hertzian loading is considered. The solution can be found [18] in terms of surface displacement (i.e., $z = 0$).

In the contact zone ($\bar{r} \leq 1$):

$$\bar{w}(\bar{r}) = \frac{1}{4}(2 - \bar{r}^2) \tag{3}$$

$$\bar{u}(\bar{r}) = -\frac{(1-2\nu)}{(1-\nu)}\frac{1}{3\pi\bar{r}}(1 - (1-\bar{r}^2)^{3/2})\frac{\bar{x}}{\bar{r}} \tag{4}$$

$$\bar{v}(\bar{r}) = -\frac{(1-2\nu)}{(1-\nu)}\frac{1}{3\pi\bar{r}}(1 - (1-\bar{r}^2)^{3/2})\frac{\bar{y}}{\bar{r}} \tag{5}$$

In the center of the contact ($\bar{r} = 0$):

$$\bar{\sigma}_{xx} = \bar{\sigma}_{yy} = (1 + 2\nu)/2 \tag{6}$$

On the edge of the contact ($\bar{r} = 1$):

$$\bar{\sigma}_{xx} = (1 - 2\nu)/3 \tag{7}$$

$$\bar{\sigma}_{yy} = -\bar{\sigma}_{xx} \tag{8}$$

With : $\bar{x} = x/a_0,\ \bar{y} = y/a_0,\ \bar{r} = \sqrt{\bar{x}^2 + \bar{y}^2},\ \bar{u} = u/\delta_0, \bar{v} = v/\delta_0, \bar{w} = w/\delta_0, \bar{\sigma}_{xx} = \sigma_{xx}/P_{h0}, \bar{\sigma}_{yy} = \sigma_{yy}/P_{h0}$.

The mean error is defined as $\eta = \left\|w_{\text{ana}} - w_{\text{app}}\right\|_1$, where w_{ana} and w_{app} are, respectively, the analytical and the approximate numerical solutions of the vertical displacement calculated at each surface point. This error is plotted versus the mesh size in Fig. 2.

This curve shows a slope of 3.5 which is close to the expected second order convergence speed value of 4. The difference

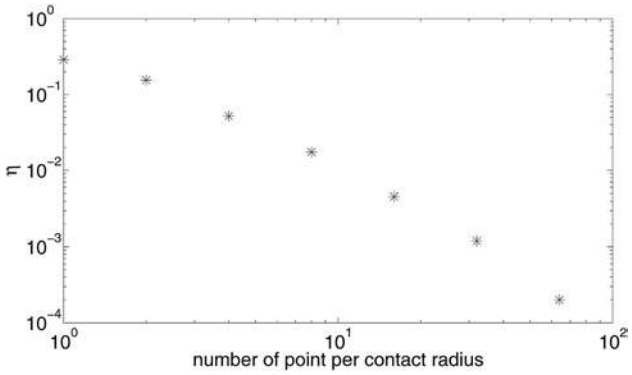

Fig. 2 Surface displacement error

is probably due to the stress singularity at the edge of the contact. Our results are in a very good agreement with the exact solution. An accuracy better than 10^{-3} is obtained using a mesh size of 1/32.

3.2 Contact Solution Using MG. The numerical relation between the displacement w at point M due to a point loading at a different point N gives the influence coefficients which can be applied in a contact algorithm [22]. This algorithm has successfully addressed rough homogeneous contact problems. Combining this algorithm with MG numerical coefficients allows us to numerically solve contact problems involving materials with varying properties throughout the depth. A spherical indenter pressed normally against a half-space is considered. The contact pressure is numerically determined and compared to the analytical Hertzian solution. The relative error ψ between the maximum Hertzian pressure P_{h0} and the numerical one is plotted as a function of the number of grid points in Fig. 3. An accuracy of 10^{-3} is reached for a grid spacing smaller than 1/32. This result validates the use of the numerical influence coefficients within the MG framework.

3.3 Contact Solution for Coatings With Graded Elastic Properties Through the Depth. Giannakopoulos and Suresh [9] gave approximate analytical solutions for both the dimensionless pressure distribution and contact half-width for a spherical rigid (parabolic) indenter pressed against a material with a specific Young's modulus variation with depth. E is varying according to an exponential law: $E(\bar{z}) = \pi e^{\bar{\alpha}\bar{z}}$, with $\bar{\alpha} = a_0\alpha$ and $\bar{z} = z/a_0$, $\nu = 0$.

$$\bar{p}(r) \approx \sqrt{1-\bar{r}^2} \quad \text{for} \quad 0 \le r \le a \tag{9}$$

$$\bar{a}^3 \approx \left(1 + \frac{C_1\bar{\alpha}^3}{3}\right)^{-1} \tag{10}$$

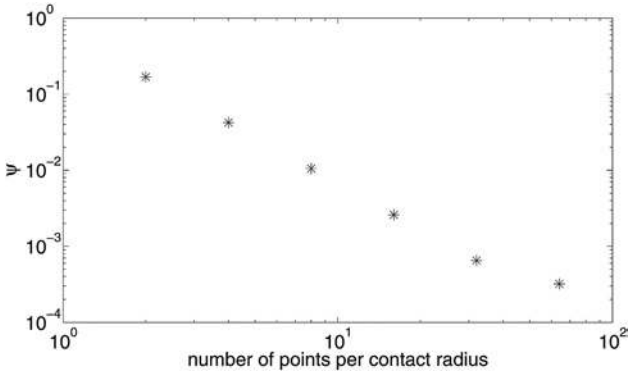

Fig. 3 Relative error in the maximum Hertzian pressure

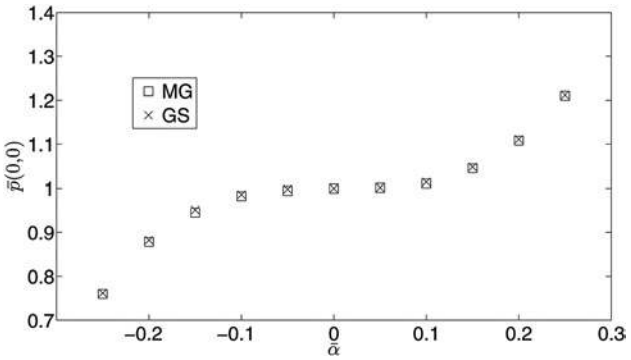

Fig. 4 Comparison between analytical (GS) and numerical (MG) dimensionless central pressure $\bar{p}$ (0,0) using the exponential law

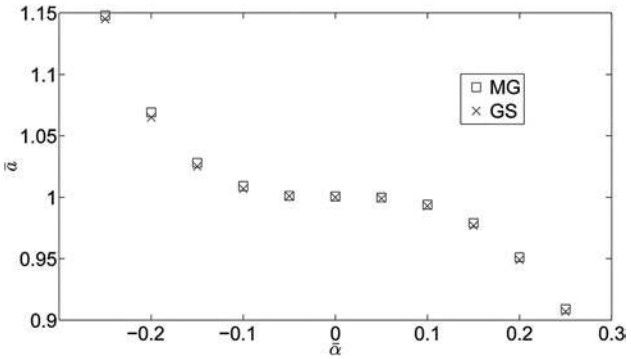

Fig. 5 Comparison between analytical (GS) and numerical (MG) dimensionless contact radius $\bar{a}$ using the exponential law

With $\bar{p}(r) = p(r)/p_{h0}$ and $\bar{a} = a/a_0$. Note that $\alpha = 0$ corresponds to the Hertzian case. The C_1 value is determined and stability issues concerning the exponential law case are described in Ref. [23].

For these conditions, MG calculations were performed for $-0.25 \le \bar{\alpha} \le 0.25$. The maximum contact pressure and contact half-width are compared to the reference values given by equations (9) and (10) and plotted in Figs. 4 and 5.

The error is of the order of one percent independently of the value of $\bar{\alpha}$. It is thus shown that the agreement between analytical and numerical solutions is excellent, validating, therefore, the ability of the MG model to address materials with property gradations versus depth. The next section is devoted to the analysis of the influence of the in-depth gradation on the internal stress field with a particular interest to the coating/substrate.

4 Results

In Fig. 6, a half cube of finite dimensions $L_x = L_y = 2 * L_z$ is shown. The Poisson's ratio is $\nu_s = \nu_c$ in the substrate and in the coating. The Young's modulus in the substrate is also assumed constant and its value is E_s. The layer is either considered with constant Young's modulus throughout the thickness (called a coating) leading to a discontinuity in material constant across the coating/substrate interface, or with a specific gradient in E_c (linear, sinusoidal…) resulting in a continuous variation in material constant across the interface. A spherical indenter is pressed on the domain with a certain load Q. The contact problem is solved numerically using the MG numerical influence coefficients and the contact algorithm. In the first subsection, coated materials are

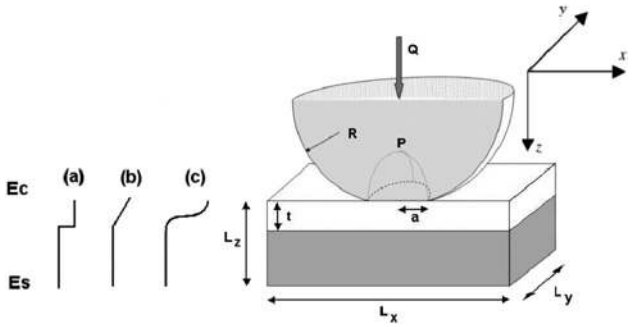

Fig. 6 Rigid spherical punch pressed against (*a*) a coating/substrate system, (*b*) a linear graded layer/substrate system, and (*c*) a sinusoidal graded layer/substrate system

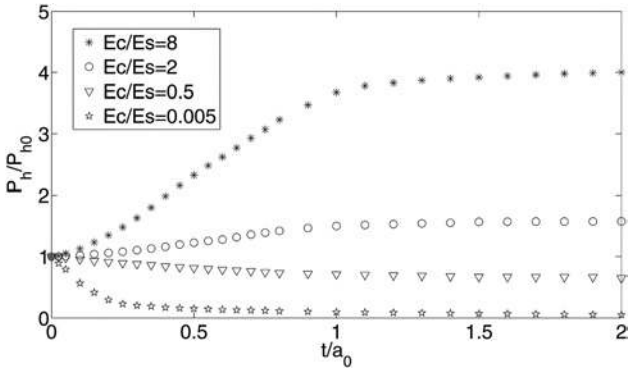

Fig. 7 Normalized contact pressure as a function of normalized layer thickness for several E_c/E_s values

studied. In a following subsection, it will be shown how graded materials can reduce mechanical damage.

4.1 Coated Materials. In this subsection, results obtained by the MG solver for coated materials are outlined. First, the algorithm performance is analyzed through a parametric study describing the influence of layer thickness ($0.01 < t/a < 10$) and mechanical properties ($0.005 < E_c/E_s < 10$) of the coating on the contact parameters (P_h, a). This problem has been studied previously by Plumet and Dubourg [3] using discrete transforms for a smaller parameter range ($0.5 < E_c/E_s < 3$). Fretigny and Chateauminois [14] calculated the stress and displacement for a rigid axisymmetric punch, assuming zero friction. They studied compliant coatings ($0.01 < E_c/E_s < 0.1$) with varying Poisson coefficients. Figure 7 shows some results obtained using the MG solver. Calculations have been performed using up to eight levels in order to have more than 10 points within coating thicknesses. Three or four global levels are used before local refinement is used. This ensures the solution accuracy to correctly capture the strong displacement gradients. The bulk size depends on the coating compliance in order to determine the complete contact area: for a large t/a_0 ratio, the contact radius tends to $(E_s/E_c)^{1/3}$. The domain size can vary between $8L_x/a$ * $8L_y/a$ * $4L_z/a$ for a stiff coating to $64L_x/a$ * $64L_y/a$ * $32L_z/a$ for compliant ones. For the calculation, one uses $h = 1$ on the coarsest grid: this configuration gives up to 513 points (eight levels) in the contact area in each direction.

The key feature of the Local Multigrid (LMG) coating model is its ability to handle both small t/a_0 ratios (0.01 - 10) and large E_c/E_s ratios (0.005 - 10).

Using the displacement obtained using the MG algorithm, the stress field within the bulk is computed separately for the coating and the substrate. Two loading conditions are considered, a normal ($f = 0$) and a sliding contact ($f = 0.3$). The stresses are plotted in Figs. 8 and 9 for $t/a_0 = 0.5$, $E_c/E_s = 3$ and for $f = 0$ and $f = 0.3$,

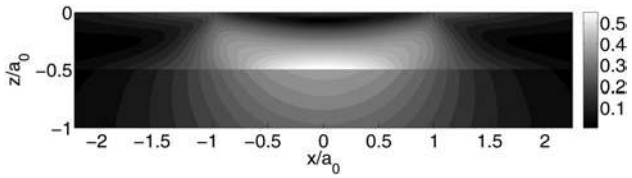

Fig. 8 $\bar{\sigma}_{VM}$ for a coated material, $E_c/E_s = 3$, normal loading, $t/a_0 = 0.5$

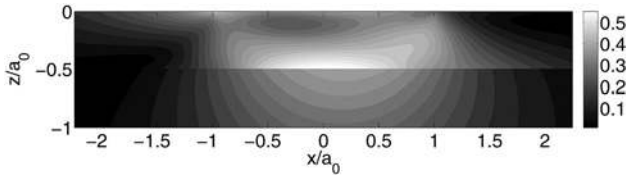

Fig. 9 $\bar{\sigma}_{VM}$ for a coated material, $E_c/E_s = 3$, normal and tangential loading $f = 0.3$, $t/a_0 = 0.5$

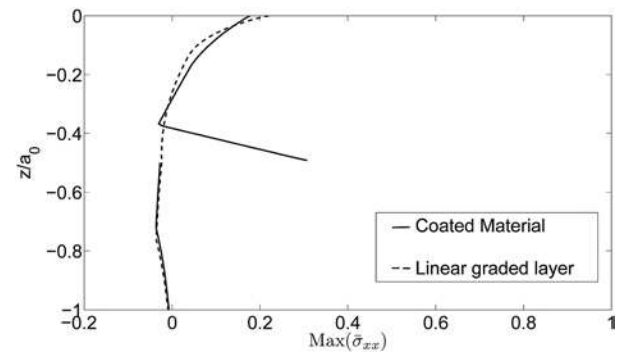

Fig. 10 Max($\bar{\sigma}_{xx}$), $t/a_0 = 0.5$ − $f = 0$

respectively. These figures highlight the Von Mises stress discontinuity at the coating-substrate interface. The material property mismatch at the interface generates a discontinuity in tensile stresses, generating debonding and/or delamination risks. These discontinuities are known to increase as E_c/E_s increases. Furthermore, the use of stiff coatings leads to a Von Mises stress increase. A smooth transition from the coating free surface to the coating/substrate interface reduces the stress concentration and leads to higher cracking resistance.

4.2 Graded Layers. The use of a graded material is a way to reduce the stress discontinuity, limit interfacial problems and thus enhance the resistance against cracking and debonding [23]. A linear variation of the Young's modulus within the coating thickness is first considered. A layer of thickness ($t/a_0 = 0.5$) is considered. Its Young's modulus varies linearly from $E_c/E_s = 3$ at the top surface to $E_c/E_s = 1$ at the interface (graded material). The reference is a coated substrate with constant Young's modulus through the thickness ($E_c/E_s = 3$).

Both normal contact ($f = 0$) and sliding contact ($f = 0.3$) are considered. Calculations are performed using the discretization described in Sec. 4.1. Under these conditions, one obtains 65 points within the depth of the layer (i.e. $0 \leq z \leq 0.5$). The maximum tensile stress $\bar{\sigma}_{xx}$ versus depth is plotted in Figs. 10 and 11 for $f = 0$ and $f = 0.3$, respectively. Von Mises stress $\bar{\sigma}_{VM}$ in the plane (x, $y = 0$, z) is plotted in Figs. 12 and 13 for the same loading conditions.

Figures 10 and 11 show a rather strong discontinuity of the tensile stress at the interface for the coated case. Please note that the maximum value is positive (traction) and its amplitude is

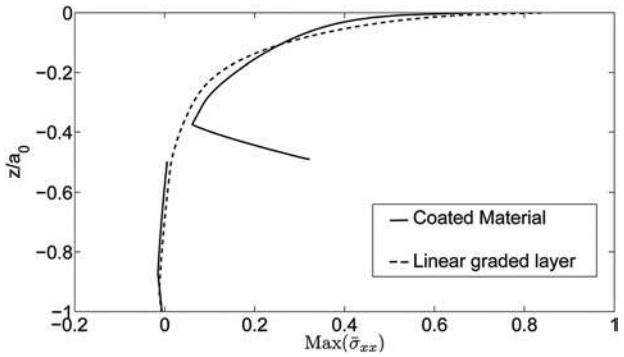

Fig. 11 Max($\bar{\sigma}_{xx}$), $t/a_0 = 0.5 - f = 0.3$

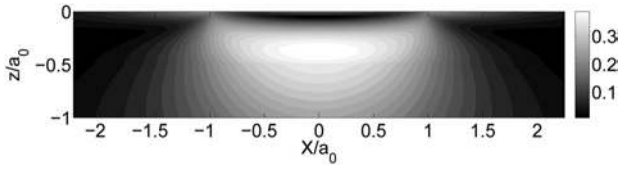

Fig. 12 $\bar{\sigma}_{VM}$ for a linear graded layer, $E_c/E_s = 3$, normal loading, $t/a_0 = 0.5$

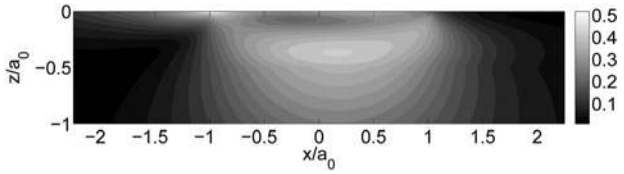

Fig. 13 $\bar{\sigma}_{VM}$ for a linear graded layer, $E_c/E_s = 3$, normal and tangential loading $f = 0.3$, $t/a_0 = 0.5$

approximately $0.3 * P_{h0}$, meaning that there is a strong tensile effect at the interface vicinity, that can lead to cracking. At the top free surface, friction increases the stresses as shown in Fig. 11. The comparison of Figs. 12 and 13 to Figs. 8 and 9 shows how the linear Young's modulus gradation acts on the Von Mises stress: a significant decrease in the maximum value is obtained and the discontinuity at the interface vanishes. The use of a graded layer, with a high Young's modulus at the top surface, improves the tribological performances and the wear resistance without inducing tensile stresses at the layer/substrate interface (see Fig. 10). Consequently, this solution may limit the occurrence of cracks at the interface while maintaining the top surface protection under normal and sliding contact.

This 3D multigrid solver can thus aid to design the coating structure by defining the gradient property to tailor performance requirements for an intended application. Moreover, all types of graded properties can be considered.

To get a deeper understanding of the property gradation role, the influence of gradients in Young's modulus on the cracking risk and the Von Mises resistance under normal contact are studied. A sinusoidal variation is used to represent a controlled change in Young's modulus over the depth t of the layer, from the top surface to the interface.

A three layer configuration is considered (Fig. 14): at the top surface, a layer of thickness $t - l/2$ with a constant E_c value such as $E_c/E_s = 3$, an intermediate layer of thickness l with a smooth sinusoidal variation of E and a third layer of thickness $t - l/2$ of E_s value. This intermediate layer acts as an interlayer and the parameter l is defined as the transition length between the coating and the substrate. Figure 15 shows the evolution of the tensile

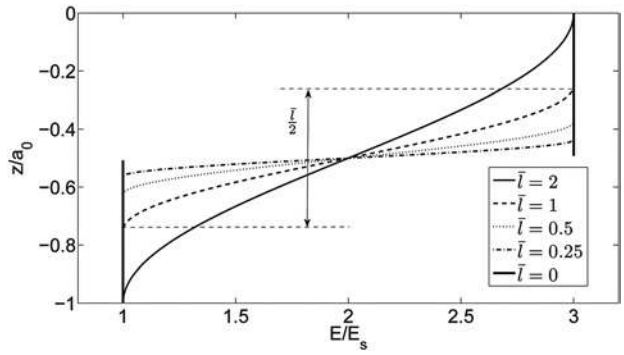

Fig. 14 Sinusoidal variation of the Young's Modulus, $E(z) = (E_s - E_c)/2 * \sin(2\pi/\bar{l} * (z/t - 1)) + (E_c + E_s)/2$

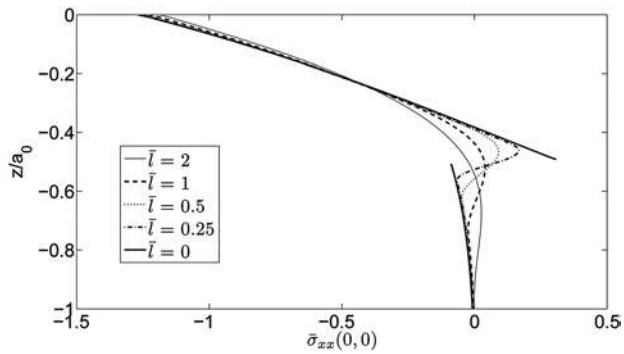

Fig. 15 $\bar{\sigma}_{xx}(x = y = 0)$, $t/a_0 = 0.5 - f = 0$ - for a sinusoidal variation (Fig. 14)

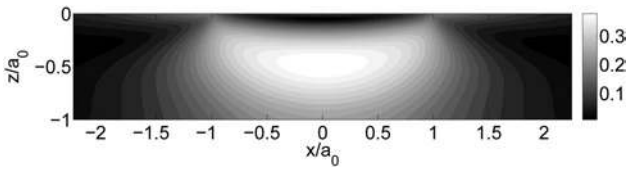

Fig. 16 $\bar{\sigma}_{VM}$ in the case of a sinusoidal variation, $t/a_0 = 0.5 - f = 0 - \bar{l} = 2$

stress $\bar{\sigma}_{xx}(x = y = 0)$ versus depth. A smooth behavior of the tensile stress within the bulk is obtained with peak values located at the top surface. At the interlayer, the discontinuity vanishes and the tensile stresses in the coating and in the substrate decrease as the dimensionless parameter $\bar{l} = l/t$ (which characterizes the transition) increases. The dimensionless Von Mises stress $\bar{\sigma}_{VM}$ is plotted in Fig. 16 for $l/t = 2$. The comparison with Von Mises variations obtained for the coated (Fig. 8) and the linear graded (Fig. 12) cases highlights the benefits of the gradation in properties. The coated case is obviously the most detrimental configuration.

4.3 Discussion on Precision. To close this section, numerical results are briefly presented. A convergence study similar to the one conducted in Sec. 2.4 was carried out for these three specific property gradations: constant, linear, and sinusoidal. The accuracy of the solver versus the number of refined levels was studied. The maximum of the relative error on the displacements was calculated and is given in Table 2.

The results are similar to the ones obtained for the homogeneous cases. The elastic property evolution does not reduce the solver efficiency.

Table 2 Maximum error $\|u_{ref} - u_{app}\|_\infty$ versus the number of refined levels for the different gradations

p	Coated	Linear graded	Sinus. graded
1	$7.82 * 10^{-5}$	$7.25 * 10^{-5}$	$6.38 * 10^{-5}$
2	$2.85 * 10^{-4}$	$2.5 * 10^{-4}$	$1.74 * 10^{-4}$
3	$7.54 * 10^{-4}$	$6.02 * 10^{-4}$	$4.0 * 10^{-4}$
4	$1.23 * 10^{-3}$	$1.13 * 10^{-3}$	$8.23 * 10^{-4}$
5	$2.35 * 10^{-3}$	$2.27 * 10^{-3}$	$1.07 * 10^{-3}$
6	$4.07 * 10^{-3}$	$3.88 * 10^{-3}$	$1.71 * 10^{-3}$

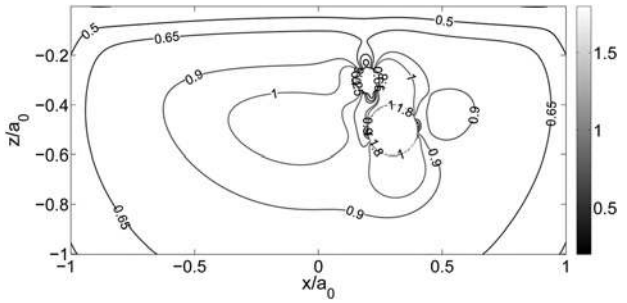

Fig. 17 $\bar{\sigma}_{VM}$ in a homogeneous bulk with a soft ($E_{inc1} = 0.01E$) and a hard ($E_{inc2} = 5E$) inclusion, $L_x/a = L_y/a = 2 * L_z/a = 8$, eight levels used: refinement strategy starting from the sixth one

4.4 Discussion on Computational Efficiency. The authors have attempted to compare the multigrid code efficiency with a commercial finite element code. The calculations were performed on similar PCs. The largest finite element solid mechanics calculation contained 10M points (30M DoF). The computing time was of the order of 10 h. A similar calculation using the MG code took less than 30 mins. Furthermore, the memory requirements of the commercial FE code were roughly 2000 times higher than of the MG code. The authors consider that this memory requirement might hamper large FEM calculations more than the normal computing times compared to MG methods. A comparison between FFT and MG methods applied to contact problems was performed by Sainsot and Lubrecht [22]. The paper concluded that the FFT methods had the advantage of extreme robustness and easy implementation, but required slightly higher computing times than the MG methods, partially because of the zero-padding required.

4.5 3D Spherical Inclusions. A final case is designed to show that full 3D spatial property variations can be accounted for. Two spherical inclusions of different size made from elastic solids with Young's modulus and Poisson's ratio (a compliant and a stiff one) are embedded within an elastically mismatched finite domain. The stress field is computed. The elastic stress and strain field due to an ellipsoidal inclusion/inhomogeneity was solved by Eshelby [24,25], and exact solutions are available for different configurations. Numerical solutions are also available. Recently, Leroux et al. [26] developed a fast method based on FFT techniques for solving contact problems when one of the mating bodies contains multiple heterogeneous inclusions. The proposed model allows one to deal with inclusions having different properties and random locations in the bulk. The case designed here aims at illustrating the model generality. Two spherical inclusions, with different radii $R_{inc1}/a_0 = 0.05$ and $R_{inc2}/a_0 = 0.1$ and elastic properties $E_{inc1} = 0.01E$ and $E_{inc2} = 5E$, are embedded within an finite elastic body. Their respective locations are:

$$(x_{inc1}/a_0 = 0.2, \quad y_{inc1}/a_0 = 0, \quad z_{inc1}/a_0 = 0.3)$$
$$(x_{inc2}/a_0 = 0.3, \quad y_{inc2}/a_0 = 0, \quad z_{inc2}/a_0 = 0.5)$$

A Hertzian pressure is imposed at the top free surface of a rectangular domain ($L_x/a = L_y/a = 2 * L_z/a = 8$). Eight grid levels are used for the computation. The refinement strategy produces three refined local levels, from the sixth to the eighth. The coarse grid involves 9*9*5 points and the finest one 257*257*129 points with a mesh size of 1/128. The total computing time is 15 mins on a PC. Inclusions 1 and 2 are modeled with more than 70,000 and 8000 points, respectively.

The Von Mises stress is plotted in Fig. 17. The influence of the inclusions on the global stress field and their interaction are clearly visible. This application outlines that any inclusion shape can be modeled as well as any property gradation within the inclusion. Furthermore, this is performed at a reduced computational cost whereas a large number of discretization points are considered.

5 Conclusion and Future Research

A 3D elastic model for heterogeneous materials is presented based on the Lamé equation for nonhomogeneous media (Eq. (1)). These equations are discretized using second order finite differences. Multigrid techniques combined with a local refinement strategy allow us to solve this problem with a limited computing cost together with a high resolution. The proposed model is validated by comparing numerical results with Hertzian solutions. A comparison with literature results [3] shows the ability of the model to address coating/substrate systems with thin layers and with large difference in substrate and coating mechanical property. An excellent agreement is obtained. Furthermore, this 3D model allows one to deal with larger property ranges E_c/E_s.

Numerical applications were then presented to illustrate the possibilities of the model. Two types of graded materials were studied, linear and sinusoidal Young's modulus variations throughout the layer thickness and its influence on the stress fields. The replacement of the property discontinuity across the coating/substrate interface by a continuous transition decreases the stress concentration at the interface and improves the material response. Furthermore, using the discretization based on finite differences, any three dimensional spatial property gradation can be addressed with a high resolution.

This is illustrated with the final case. Two spherical inclusions of different size and mechanical properties embedded within an elastic mismatched bulk is submitted to an Hertzian pressure. Despite the large number of discretization points, the computation of the stress field is fast and straightforward whatever the number, the complexity of the shape and the heterogeneity of the properties of the inclusions.

Nomenclature

E_c = Young's modulus of the coating
E_s = Young's modulus of the substrate
P_{h0} = uncoated Hertzian pressure
P_h = coated maximum pressure
h = grid spacing
a_0 = uncoated Hertzian contact radius
a = coated contact radius
t = coating thickness
i, j, k = index in x-y-z direction
u, v, w = displacements in x-y-z direction
λ, μ = Lamé coefficients
$\bar{\sigma}_{VM} = \sigma_{VM}/P_{h0}$ = dimensionless Von Mises stress
$\bar{\sigma}_{xx}, \bar{\sigma}_{yy}$ = dimensionless tensile stresses
f = friction coefficient
L_x, L_y, L_z = half cube dimensions in x-y-z direction

References

[1] Ju, Y., and Liu, S., 1988, "Parameters Affecting Thermomechanical Cracking in Coated Media Due to High Speed Friction Load," Trans. ASME J. Tribol., **110**, pp. 222–229.

[2] Leroy, J. M., Floquet, A., and Villechaise, B., 1989, "Thermomecanical Behavior of Multilayered Media: Theory," Trans. ASME J. Tribol., **111**, pp. 538–544.

[3] Plumet, S., and Dubourg, M. C., 1998, "A 3D Model for a Multilayered Body Loaded Normally and Tangentially Against a Rigid Body: Application," J. Tribol., **120**, pp. 668–676.

[4] Polonsky, I. A., and Keer, L. M., 2000, "A Fast and Accurate Method for Numerical Analysis of Elastic Layered Contacts" Trans. ASME J. Tribol., **122**, pp. 30–35.
[5] Polonsky, I. A., and Keer, L. M., 2000, "Fast Method for Solving Rough Contact Problems: A Comparative Study," Trans. ASME J. Tribol., **122**, pp. 36–41.
[6] Nogi, T., and Kato, T., 1997, "Influence of a Hard Surface Layer on the Limit of Elastic Contact: Part 1: Analysis Using a Real Surface Model," Trans. ASME J. Tribol., **119**, pp. 493–500.
[7] Kesler, O., Finot, M., Suresh, S., and Sampath, S., 1996, "Determination of Processing-Induced Stresses and Properties of Layered and Graded Coatings: Experimental Method and Results for Plasma-Sprayed Ni-Al2 03," Acta Mater., **45**, pp. 3113–3134.
[8] Suresh, S., and Mortensen, A., 1997, "Functionally Graded Metals and Metal-Ceramic Composites: Part 2 Thermomechanical Behaviour," Int. Mater. Rev., **42**, pp. 85–116.
[9] Giannakopoulos, A. E., and Suresh, S., 1996, "Indentation of Solids With Gradients in Elastic Properties: Part II. Axisymmetric Indentords," Int. J. Solids Struct., **34**, pp. 2393–2428.
[10] Prasad, A., Dao, M., and Suresh, S., 2008, "Steady-State Frictional Sliding Contact on Surfaces of Plastically Graded Materials," Acta Mater., **57**, pp. 511–524.
[11] Holmberg, K., Laukkanen, A., Ronkainen, H., Wallin, K., Varjus, S., and Koskinen, J., 2006, "Tri-Bological Contact Analysis of a Rigid Ball Sliding on a Hard Coated Surface Part II: Material Deformations, Influence of Coating Thickness and Young's Modulus," Surf. Coat. Technol., **200**, pp. 3810–3823.
[12] Ye, N., and Komvopoulos, K., 2003, "Three-Dimensional Finite Element Analysis of Elastic-Plastic Layered Me-Dia Under Thermomechanical Surface Loading," J. Tribol., **125**, pp. 52–59.
[13] Venner, C. H., and Lubrecht, A. A., 2000, *Multi-Level Methods in Lubrication*, Elsevier Tribology Series, Amsterdam.
[14] Fretigny, C., and Chateauminois, A., 2007, "Solution for the Elastic Field in a Layered Medium Under Axisymmetric Contact Loading," J. Phys. D, **40**, pp. 5418–5426.
[15] Perriot, A., and Barthel, E., 2004, "Elastic Contact to a Coated Half-Space: Effective Elastic Modulus and Real Penetration," J. Mater. Res., **19**, pp. 600–608.
[16] Watremetz, B., Baietto Dubourg, M. C., and Lubrecht, A. A., 2007, "2D Thermo-Mechanical Contact Simulations in a Functionally Graded Material: A Multigrid-Based Approach," Tribol. Int., **40**, pp. 754–762.
[17] Boffy, H., Baietto, M. C., Sainsot, P., and Lubrecht, A. A., 2012, "Detailed Modelling of a Moving Heat Source Using Multigrid Methods," Tribol. Int., **46**, pp. 279–287.
[18] Johnson, K. L., 1985, *Contact Mechanics*, Cambridge University Press, Cambridge, UK.
[19] Bai, D., and Brandt, A., 1987, "Local Mesh Refinement Multilevel Techniques," J. Sci. Comput., **8**, pp. 109–134.
[20] Brandt, A., 1984, *Multigrid Techniques: Guide With Applications to Fluid Dynamics*, Gesellschaft fur Mathematik und Datenverarbeitung, Munich, Germany.
[21] Brandt, A., 1977, "Multilevel Adaptative Solution to Boundary Value Problems," Math. Comput., **31**, pp. 333–390.
[22] Sainsot, P., and Lubrecht, A. A., 2010, "Efficient Solution of the Dry Contact of Rough Surfaces: A Comparison of FFT and MG Methods," Proc. Inst. Mech. Eng., Part J: J. Eng. Tribol., **225**, pp. 441–448.
[23] Suresh, S., 2001, "Graded Materials for Resistance to Contact Deformation and Damage," Science, **292**, pp. 2447–2451.
[24] Eshelby, J. D., 1957, "The Determination of the Elastic Field of an Ellipsoidal Inclusion, and Related Problems," Proc. R. Soc. London, **241**, pp. 376–396.
[25] Eshelby, J. D., 1959, "The Elastic Field outside an Ellipsoidal Inclusion," Proc. R. Soc. London Ser. A, **252**, p. 561.
[26] Leroux, J., Fulleringer, B., and Nélias, D., 2010, "Contact Analysis in Presence of Spherical Inhomogeneities Within a Half-Space," Int. J. Solids Struct., **47**, pp. 3034–3049.